ACS APPLIED MATERIALS & INTERFACES

Research Article

www.acsami.org

Yolk Bishell $Mn_xCo_{1-x}Fe_2O_4$ Hollow Microspheres and Their Embedded Form in Carbon for Highly Reversible Lithium Storage

Zailei Zhang,*[,†] Yongjun Ji,[†] Jing Li,[†] Qiangqiang Tan,*[,†] Ziyi Zhong,[‡] and Fabing Su*[,†]

[†]State Key Laboratory of Multiphase Complex Systems, Institute of Process Engineering, Chinese Academy of Sciences, Beijing 100190, China

[‡]Institute of Chemical Engineering and Sciences, A*star, 1 Pesek Road, Jurong Island, Singapore 627833

Supporting Information

ABSTRACT: The yolk−shell hollow structure of transition metal oxides has many applications in lithium-ion batteries and catalysis. However, it is still a big challenge to fabricate uniform hollow microspheres with the yolk bishell structure for mixed transition metal oxides and their supported or embedded forms in carbon microspheres with superior lithium storage properties. Here we report a new approach to the synthesis of manganese cobalt iron oxides/carbon ($Mn_xCo_{1-x}Fe_2O_4$ ($0 \le x \le 1$)) microspheres through carbonization of $Mn^{2+}Co^{2+}Fe^{3+}$/carbonaceous microspheres in N_2, which can be directly applied as high-performance anodes with a long cycle life for lithium storage. Furthermore, uniform hollow microspheres with a $Mn_xCo_{1-x}Fe_2O_4$ yolk bishell structure are obtained by annealing the above $Mn_xCo_{1-x}Fe_2O_4$/carbon microspheres in air. As demonstrated, these anodes exhibited a high reversible capacity of 498.3 mAh g^{-1} even after 500 cycles for $Mn_{0.5}Co_{0.5}Fe_2O_4$/carbon microspheres and 774.6 mAh g^{-1} over 100 cycles for $Mn_{0.5}Co_{0.5}Fe_2O_4$ yolk bishell hollow microspheres at the current density of 200 mA g^{-1}. The present strategy not only develops a high-performance anode material with long cycle life for lithium-ion batteries but also demonstrates a novel and feasible technique for designed synthesis of transition metal oxides yolk bishell hollow microspheres with various applications.

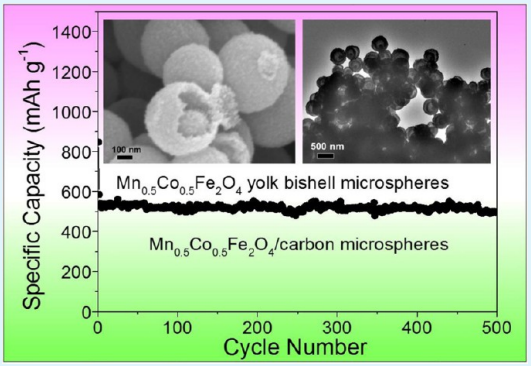

KEYWORDS: *manganese cobalt iron oxides, yolk bishell, hollow microspheres, anode, lithium-ion batteries*

1. INTRODUCTION

In recent years there have been increasing concerns on environmental pollution due to the accelerated consumption and depletion of the nonrenewable fossil-fuels.[1,2] Because of the good sustainability, environmental benignity and safety, high energy density and long cycle life, and great potentiality for applications in potable electronics, electric vehicles, and renewable energy storage, lithium-ion batteries (LIBs) have attracted tremendous attentions in these years.[3−6] Recently, a variety of transition metal oxides (TMOs) structures, such as hollow Fe_3O_4 nanospheres,[7] porous nanostructured Co_3O_4,[8] hollow MnO nanospheres,[9] hollow $CoMn_2O_4$ spheres,[10] and mesoporous $MnFe_2O_4$ microspheres,[11] have been demonstrated as the promising high-performance anode materials for LIBs because of their much higher lithium storage capacities and safety than that of commercially used graphite.[12−14] Furthermore, the prepared TMOs/carbon composites, for instance, Fe_3O_4 nanoparticles embedded in porous carbon matrix,[15] mesoporous carbon nanotubes filled with Co_3O_4 nanoparticles,[16] hollow porous MnO/carbon microspheres,[17] yolk−shell ZnO-C microspheres,[18] hierarchical and porous ZnO−Ag-C microspheres,[19] mesoporous $CoFe_2O_4$ nanospheres/carbon nanotubes,[20] and carbon-coated $CoMn_2O_4$ triple-shelled hollow spheres,[21] cannot only accommodate the volume change during the discharge−charge processes but also provide stable electrical and ionic transfer channels, resulting in better cyclic stability than bare TMOs.[22−24]

More recently, significant efforts have been devoted to the fabrication of these yolk−shell hollow microspheres which can be used in a wide range of areas including nanoreactor, catalyst, drug delivery, solar cells, and LIBs.[25−31] Various metal oxides with yolk−shell hollow nanostructures have been synthesized on the basis of the Kirkendall and Ostwald ripening effect,[32,33] and of the sacrificial template methods.[34−36] The general route for sacrificial template synthesis of nanostructured hollow materials includes the following steps: template preparation (such as carbonaceous spheres, silica spheres, or polystyrene spheres), directed synthesis and assembling of the targeted materials over the template, and removal of the template.[37,38] For example, hollow TiO_2 spheres[39] and hollow Fe_2O_3 spheres[40] were prepared by using polystyrene spheres as the template; hollow Co_3O_4 spheres[41] and hollow manganese oxide nanospheres[42] were synthesized using the silica spheres template; hollow NiO nanospheres,[43] hollow Fe_2O_3 micro-

Received: January 20, 2015
Accepted: March 4, 2015
Published: March 4, 2015

DOI: 10.1021/acsami.5b00617
ACS Appl. Mater. Interfaces 2015, 7, 6300−6309

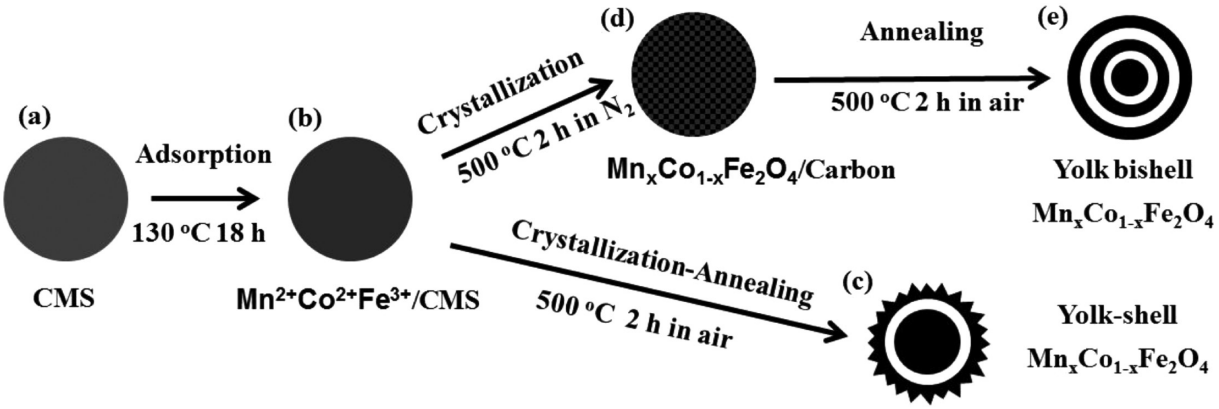

Figure 1. Schematic illustration of the formation processes for the carbonaceous microspheres (CMS) (a), $Mn^{2+}Co^{2+}Fe^{3+}$/CMS microspheres (b), $Mn_xCo_{1-x}Fe_2O_4$ ($0 \le x \le 1$) yolk−shell hollow microspheres (c), $Mn_xCo_{1-x}Fe_2O_4$/carbon microspheres (d), and $Mn_xCo_{1-x}Fe_2O_4$ yolk bishell hollow microspheres (e).

spheres,[44] and hollow $NiFe_2O_4$ spheres[45] were prepared using the carbonaceous spheres template. Recently Lou's group has developed a strategy to the synthesis of carbon-coated $CoMn_2O_4$ triple-shelled hollow spheres using the carbonaceous spheres template, which exhibit a specific capacity of 726.7 mAh g^{-1} after 200 cycles at a current density of 200 mA g^{-1}.[21] Wang and his co-workers synthesized triple-shelled Co_3O_4 hollow microspheres through sacrificing the carbonaceous sphere template and observed a specific capacity as high as 1615.8 mAh g^{-1} after 30 cycles at a current density of 50 mA g^{-1}.[46] However, it still remains as a great challenge for the formation of uniform transition metal oxide complex hollow microspheres with a yolk bishell structure and mixed transition metal oxides/carbon microspheres for LIBs with a long cycling life from carbonaceous spheres template.[47]

Inspired by but differing from the previous work using adsorption and annealing processes for the synthesis of hollow microspheres, here we report the synthesis of $Mn_xCo_{1-x}Fe_2O_4$ ($0 \le x \le 1$) yolk bishell hollow microspheres, including $MnFe_2O_4$, $CoFe_2O_4$, $Mn_{0.25}Co_{0.75}Fe_2O_4$, $Mn_{0.5}Co_{0.5}Fe_2O_4$, and $Mn_{0.75}Co_{0.25}Fe_2O_4$, based on the general "adsorption, crystallization, and annealing" processes, a strategy not reported previously. Remarkably, the prepared $Mn_{0.5}Co_{0.5}Fe_2O_4$/carbon microspheres with $Mn_{0.5}Co_{0.5}Fe_2O_4$ nanoparticles homogeneously embedded in the carbon network after the one-pot carbonization of $Mn^{2+}Co^{2+}Fe^{3+}$/carbonaceous spheres exhibit superior lithium storage properties (a high capacity of 498.3 mAh g^{-1} at 200 mA g^{-1} even after 500 cycles). This work paves a new way for fabrication of hollow microspheres with transition metal oxides yolk bishell and utilization of transition metal oxides/carbon microspheres as anodes for LIBs with long cycling life.

2. EXPERIMENTAL SECTION

2.1. Material Synthesis. In a typical synthesis, carbonaceous microspheres (CMS) were first synthesized by a modified hydrothermal method reported previously.[48] Glucose (12 g, Sinopharm Chemical Reagent Co., Ltd.) was dissolved in deionized water (70 mL) and glycol (5 mL) to form a homogeneous slurry, which was subsequently sealed in a stainless-steel autoclave and heated at 180 °C for 24 h. The CMS were collected by centrifugation, washed with distilled water and absolute ethanol, and finally dried in vacuum at 80 °C for 24 h. Subsequently, 100 mg of CMS was added into 100 mL of glycol followed by sonication to reach a high dispersion. After that, $Co(CH_3COO)_2{\cdot}4H_2O$ (0.5 mmol), $Mn(CH_3COO)_2{\cdot}4H_2O$ (0.5 mmol), and $FeCl_3{\cdot}6H_2O$ (2.0 mmol) were added into the above mixture with stirring. The obtained mixture was then transferred into a round-bottom flask and kept refluxing at 130 °C for 18 h in an oil bath, followed with a natural cooling down to room temperature. The product ($Mn^{2+}Co^{2+}Fe^{3+}$/CMS) was collected by centrifugation and washed with ethanol. In order to obtain $Mn_{0.5}Co_{0.5}Fe_2O_4$ yolk−shell hollow microspheres, the $Mn^{2+}Co^{2+}Fe^{3+}$/CMS product was further annealed in air at 500 °C for 2 h with a slow heating rate of 2 °C min^{-1}. The $Mn_{0.5}Co_{0.5}Fe_2O_4$/carbon microspheres were prepared by annealing the $Mn^{2+}Co^{2+}Fe^{3+}$/CMS at 500 °C in high-purity N_2 for 2 h with a slow heating rate of 2 °C min^{-1}. Finally, the $Mn_{0.5}Co_{0.5}Fe_2O_4$ yolk bishell hollow microspheres were obtained by annealing the $Mn_{0.5}Co_{0.5}Fe_2O_4$/carbon microspheres at 500 °C in air for 2 h with a slow heating rate of 2 °C min^{-1}.

2.2. Materials Characterization. X-ray diffraction patterns (XRD) were recorded on a PANalytical X'Pert PRO MPD using the Cu Kα radiation (λ = 1.5418 Å). The microscopic feature of the samples was characterized by field-emission scanning electron microscopy (FESEM) with an energy-dispersive X-ray spectrometer (EDX) (JSM-7001F, JEOL, Tokyo, Japan) and transmission electron microscopy (TEM) with an EDX (JEM-2010F, JEOL, Tokyo, Japan) operated at 300 kV. Thermogravimetric (TG) analysis was carried out on an EXSTAR TG/DTA 6300 (Seiko Instruments, Japan) at a heating rate of 2 °C min^{-1} in air. The elemental analysis was conducted by inductively coupled plasma optical emission spectrometry (ICP-OES, Optima 5300DV, Pekin Elmer). The pore nature of the samples was investigated using physical adsorption of N_2 at the liquid-nitrogen temperature (−196 °C) on an automatic volumetric sorption analyzer (NOVA3200e, Quantachrome). Prior to the measurement, the sample was degassed at 200 °C for 12 h under vacuum. The specific surface area was determined according to the Brunauer−Emmett−Teller (BET) method in the relative pressure range of 0.05−0.2. X-ray photoelectron spectroscopy (XPS) analysis was carried out on an ESCALAB 250Xi from Thermo Scientific Corporation using Al_{Ka} X-ray radiation.

2.3. Electrochemical Measurement. The working electrode was prepared by mixing the active materials, acetylene black, and polyvinylidene fluoride (PVDF) in a weight ratio of 80:10:10 with *N*-methylpyrrolidone (NMP) as a solvent. The resulting slurries were cast onto a common Cu foil (current collector). The film composed of Cu foil and slurries were rolled into 25 μm thin sheets and then dried at 50 °C for 24 h. The film were cut into disks with a diameter of 14 mm and then dried at 120 °C in vacuum for 24 h. CR2016 coin-type cells were assembled in an Ar-filled glovebox with lithium foils as the counter electrodes and polypropylene microporous films (Celgard 2400) as separators. The liquid electrolyte is 1 mol L^{-1} $LiPF_6$ in a mixture of ethylene carbonate (EC) and dimethyl carbonate (DMC) (1:1, v/v). The galvanostatic charge and discharge tests were carried out by the CT2001A LAND testing instrument in the voltage range

DOI: 10.1021/acsami.5b00617
ACS Appl. Mater. Interfaces 2015, 7, 6300−6309

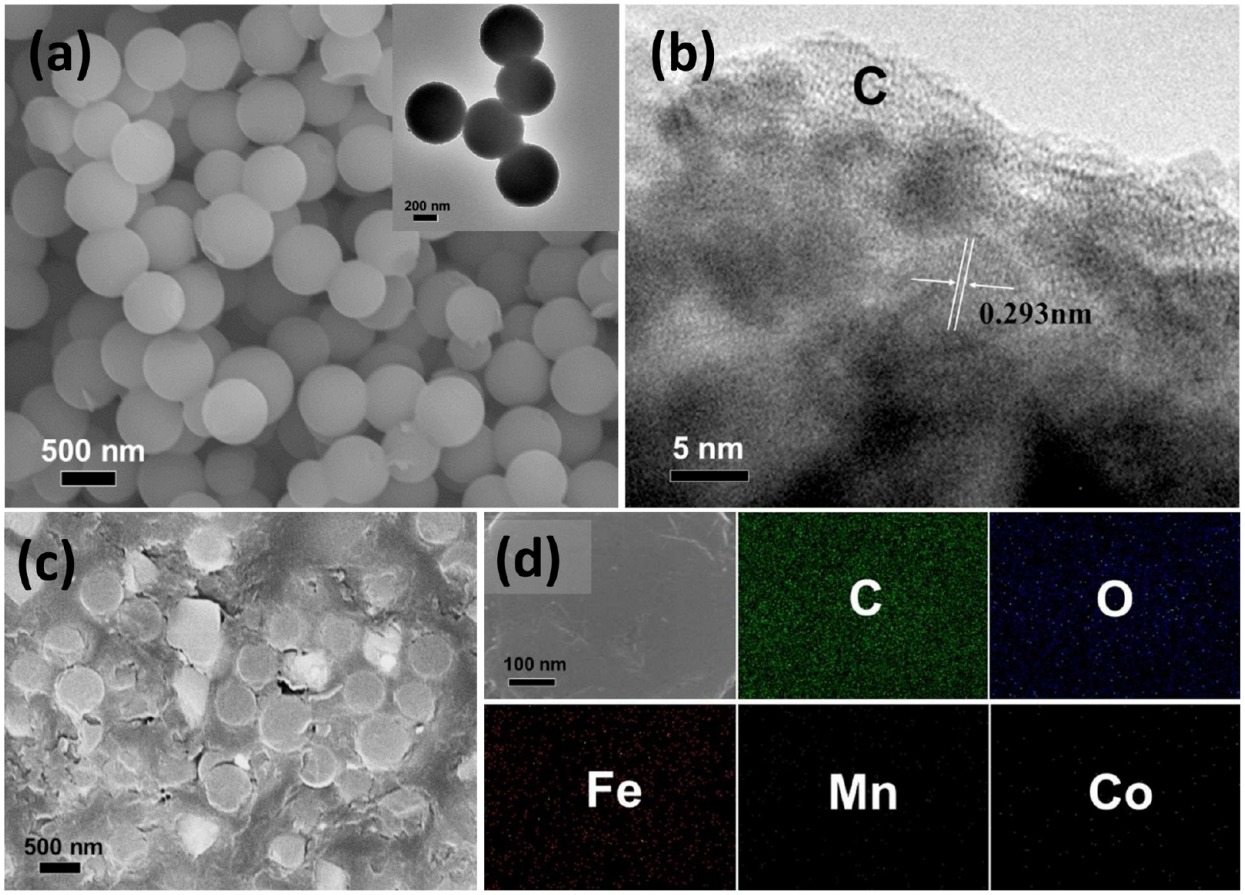

Figure 2. SEM image (a) (inset is its TEM image), HRTEM image (b), cross-sectional SEM image (the back scattered image recorded both in the secondary electron image and back scattered electron detector) (c), and corresponding elemental mapping images of C, Fe, Mn, Co, and O of $Mn_{0.5}Co_{0.5}Fe_2O_4$/carbon microspheres (d).

between 0.01 and 3.0 V at current densities of 200, 400, 1000, and 2000 mA g^{-1}. Cyclic voltammetry (CV) measurements were carried out at room temperature using a CHI660D potentiostat in the voltage range of 0−3 V at a scanning rate of 0.1 mV s^{-1}, and electrochemical impedance spectroscopy (EIS) measurements were also conducted on the same instrument over a frequency range from 100 kHz to 10 mHz with an ac oscillation of 5 mV.

3. RESULTS AND DISCUSSION

Figure 1 illustrates the formation processes of the $Mn_xCo_{1-x}Fe_2O_4$ ($0 \le x \le 1$) yolk bishell and yolk−shell microspheres and of the $Mn_xCo_{1-x}Fe_2O_4$/carbon microspheres. The reaction conditions used for synthesis of all the samples are compiled in Table S1 in the Supporting Information. First of all, carbonaceous microspheres (CMS), which contain about 88.2 wt % of carbon (Figure 1a and Figure S1a in the Supporting Information) obtained by the modified hydrothermal method[48] are well dispersed into an glycol solution of the metal precursors. The prepared CMS possess a large quantity of interior and outer surface functional groups such as −C═O and −OH, thus offering an ideal chemical environment for the adsorption of metal cations.[48,49] Subsequently, the metal precursors are added, and the solution is heated up to 130 °C in an oil bath and kept stirring and refluxing at this temperature for 18 h to form the $Mn^{2+}Co^{2+}Fe^{3+}$/CMS microspheres (Figure 1b and Figure S1b in the Supporting Information). During this process, metal glycolate will be formed by adsorbing metal precursors in both the interior and outer surface of CMS.[50] At last, the $Mn_xCo_{1-x}Fe_2O_4$ yolk−shell hollow microspheres (Figure 1c) can be prepared through a crystallization-annealing treatment in air which accompanies with release of the small molecules and functional groups during the combustion of CMS. The $Mn_xCo_{1-x}Fe_2O_4$/carbon microspheres (Figure 1d) can be easily generated through crystallization and carbonization processes in high-purity N_2 and be further transformed into the yolk bishell $Mn_xCo_{1-x}Fe_2O_4$ hollow microspheres (Figure 1e) through an annealing treatment to the former in air. In the transformation, the formation of the hollow volume should be due to the release of the small molecules and functional groups in the CMS template and the complete combustion of the CMS template. In our method, one of the important features differing from the previously reported template methods using CMS for formation of hollow microspheres is that the "crystallization" and "annealing" processes are separated. Most importantly, the prepared $Mn_xCo_{1-x}Fe_2O_4$/carbon microspheres with $Mn_xCo_{1-x}Fe_2O_4$ nanoparticles homogeneously distributed in the carbon networks showed long cycling life as anodes for LIBs. It should be pointed out that, in principle, the strategy demonstrated here can be easily extended to prepare other transition metal oxides/carbon microspheres and transition metal oxide hollow microspheres with one yolk but mutiple shells with superior lithium storage properties. For example, we can prepare transition metal oxide hollow microspheres with one yolk but multiple shells using one type of transition metal oxide/carbon microspheres as the hard template followed with repeated

DOI: 10.1021/acsami.5b00617
ACS Appl. Mater. Interfaces 2015, 7, 6300−6309

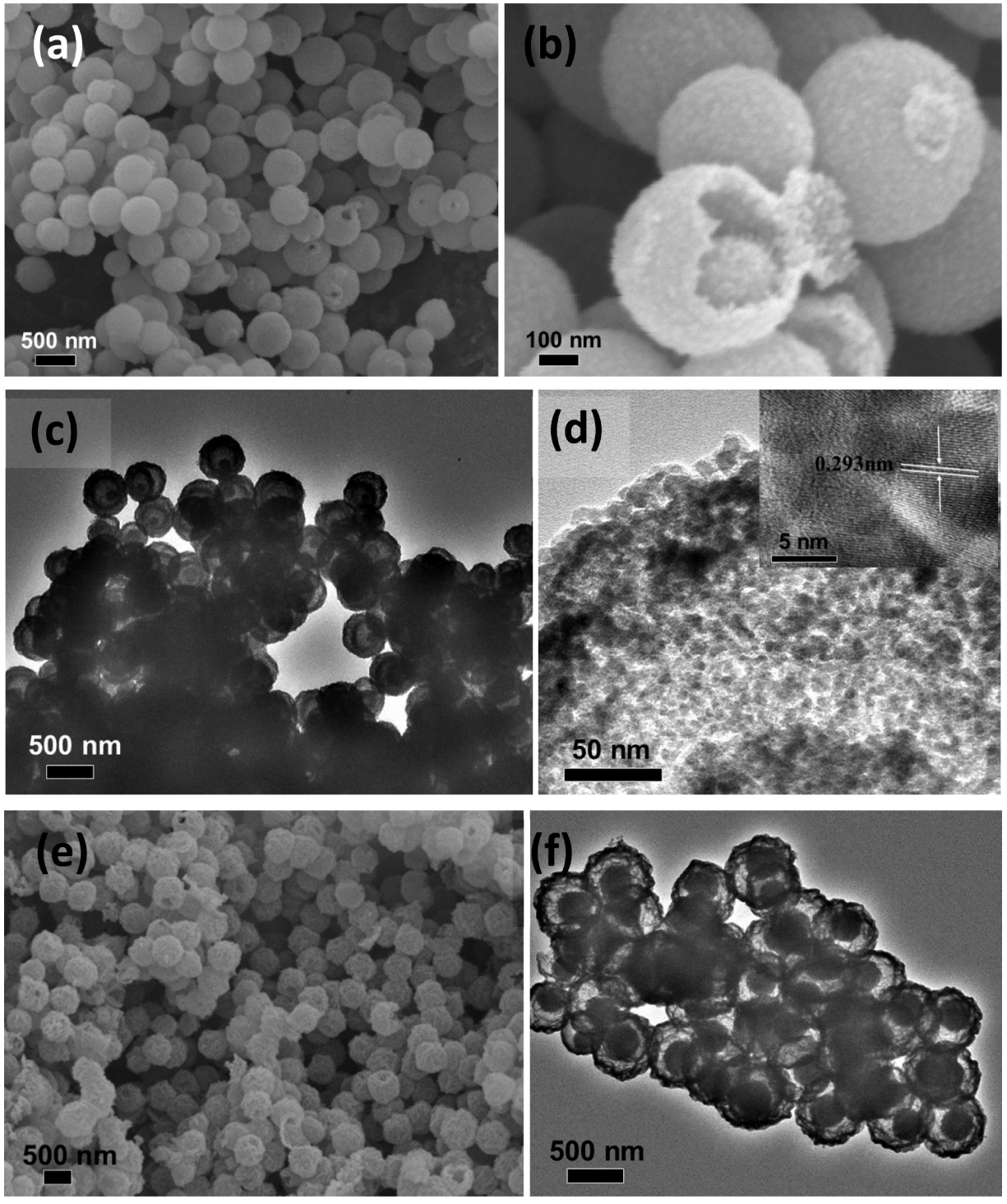

Figure 3. SEM images (a and b) and TEM images (c and d) of $Mn_{0.5}Co_{0.5}Fe_2O_4$ yolk bishell hollow microspheres (inset is its HRTEM image) after crystallization and annealing treatment and SEM (e) and TEM (f) images of $Mn_{0.5}Co_{0.5}Fe_2O_4$ yolk−shell hollow microspheres after crystallization-annealing treatment.

adsorption of another transition metal oxide and annealing treatment.

Figure S2 in the Supporting Information shows the TEM images of the Fe_2O_3 hollow microspheres, yolk−shell, and yolk bishell hollow microspheres. The thin shell Fe_2O_3 hollow microspheres with a diameter of about 400−500 nm are obtained after an 8 h-adsorption followed with a crystallization-annealing treatment (Figure S2a in the Supporting Information), or an 8 h-adsorption followed with a crystallization and then an annealing treatment (Figure S2b in the Supporting Information). Further increasing adsorption time to 14 h with the crystallization-annealing treatment (Figure S2c in the Supporting Information), or the crystallization and then annealing treatment (Figure S2d in the Supporting Information), or to 18 h with crystallization-annealing treatment (Figure S2e in the Supporting Information), Fe_2O_3 yolk−shell hollow microspheres are always obtained. Figure S2f in the Supporting Information shows the Fe_2O_3 yolk bishell hollow

DOI: 10.1021/acsami.5b00617
ACS Appl. Mater. Interfaces 2015, 7, 6300−6309

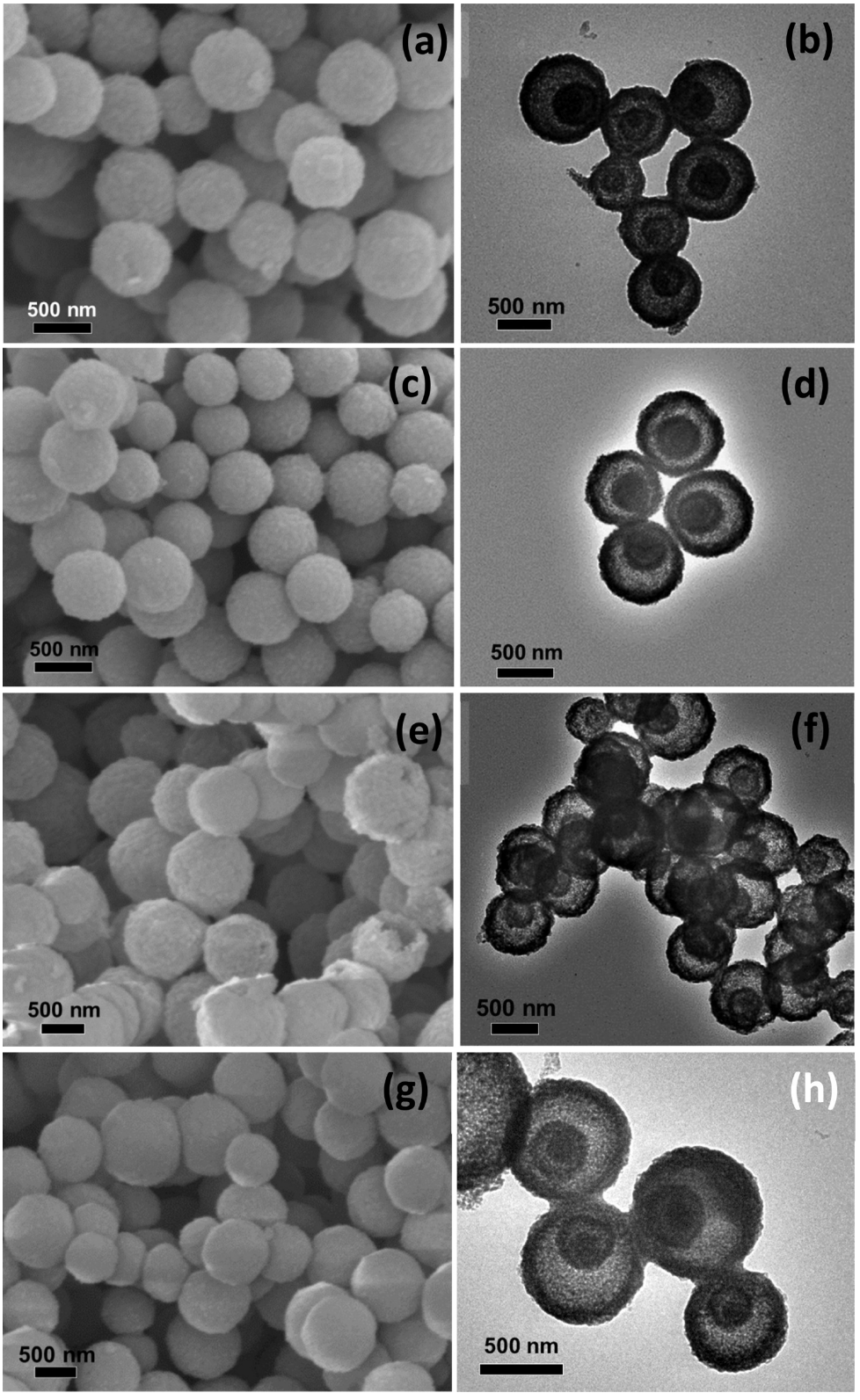

Figure 4. SEM (a, c, e, and g) and TME (b, d, f, and h) images of $MnFe_2O_4$ (a and b), $CoFe_2O_4$ (c and d), $Mn_{0.25}Co_{0.75}Fe_2O_4$ (e and f), and $Mn_{0.75}Co_{0.25}Fe_2O_4$ (g and h) yolk bishell hollow microspheres.

microspheres prepared by the 18 h-adsorption followed with the crystallization and annealing treatment. The hollow structure could be easily adjusted by changing the adsorption time in the glycol solution and the crystallization and annealing treatment parameters. The measured XRD patterns (Figure S3 in the Supporting Information) for all the Fe_2O_3 samples clearly confirm the formation of Fe_2O_3 crystallites (JCPDS card no. 33-00664).[51] The Fe_2O_3 yolk bishell hollow microspheres can be prepared after the crystallization and annealing treatment with 18 h-adsorption. However, with further increase of the

DOI: 10.1021/acsami.5b00617
ACS Appl. Mater. Interfaces 2015, 7, 6300−6309

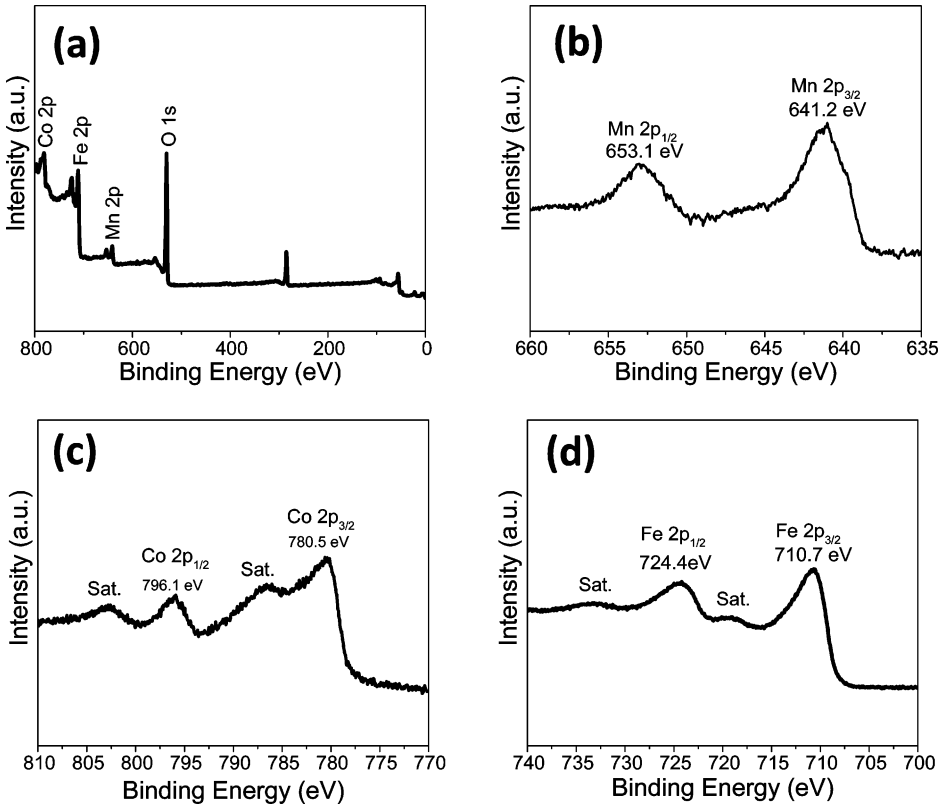

Figure 5. XPS spectra for the $Mn_{0.5}Co_{0.5}Fe_2O_4$ yolk bishell hollow microspheres: wide spectrum (a), Mn 2p (b), Co 2p (c), and Fe 2p (d).

adsorption time to 22 h (the results not shown here), the prepared Fe_2O_3 microspheres still maintain similar yolk bishell hollow structure without much change in thickness of the shell, which may be due to the reaching of the saturated adsorption of CMS in glycol solution for Fe^{3+} after the 18 h-adsorption.

The morphological and structural features of the $Mn_{0.5}Co_{0.5}Fe_2O_4$/carbon microspheres are shown in Figure 2. Both the SEM and TEM images (Figure 2a) demonstrate that uniform $Mn_{0.5}Co_{0.5}Fe_2O_4$/carbon microspheres with a diameter of about 400−500 nm were prepared through the adsorption of Mn^{2+}, Co^{2+}, and Fe^{3+} on the outer and interior surface of CMS followed with the carbonization treatment. The HRTEM image shown in Figure 2b, the cross-sectional SEM image in Figure 2c (the back scattered image recorded both in the secondary electron image and back scattered electron detector), and the corresponding elemental mapping images in Figure 2d indicate that the $Mn_{0.5}Co_{0.5}Fe_2O_4$ nanoparticles are uniformly dispersed in the carbon network. The TG curve of $Mn_{0.5}Co_{0.5}Fe_2O_4$/carbon microspheres in air shows that there is a weight loss of ~74.2 wt % from 100 to 1000 °C (Figure S4 in the Supporting Information); therefore, the content of $Mn_{0.5}Co_{0.5}Fe_2O_4$ nanoparticles in $Mn_{0.5}Co_{0.5}Fe_2O_4$/carbon microspheres is calculated to be about 25.8 wt %.

The SEM images in Figure 3a,b show that the uniform $Mn_{0.5}Co_{0.5}Fe_2O_4$ yolk−shell hollow microspheres with a size of 300−500 nm are formed after the annealing treatment for the $Mn_{0.5}Co_{0.5}Fe_2O_4$/carbon microspheres, while the TEM images in Figure 3c,d indicate that the $Mn_{0.5}Co_{0.5}Fe_2O_4$ yolk bishell hollow microspheres are composed of small nanoparticles. The HRTEM image in the inset of Figure 3d shows that the lattice fringe spacing within the nanoparticles is about 0.293 nm, corresponding to the interplanar distance of (220) planes in $Mn_{0.5}Co_{0.5}Fe_2O_4$. The SEM image, EDX spectra, and corresponding elemental mapping images of $Mn_{0.5}Co_{0.5}Fe_2O_4$ yolk bishell hollow microspheres show the homogeneous distribution of all the four elements (Mn, Co, Fe, and O) (Figure S5 in the Supporting Information). The SEM image in Figure 3e and the TEM image in Figure 3f show that $Mn_{0.5}Co_{0.5}Fe_2O_4$ yolk−shell hollow microspheres are obtained after the direct crystallization-annealing treatment to the $Mn^{2+}Co^{2+}Fe^{3+}$/CMS microspheres. Figure S6 in the Supporting Information indicates that the surface area of the $Mn_{0.5}Co_{0.5}Fe_2O_4$ yolk−shell and yolk bishell hollow microspheres is about 24.7 m^2/g and 40.4 m^2/g, respectively, probably because of the smaller size of $Mn_{0.5}Co_{0.5}Fe_2O_4$ nanoparticles forming a hollow porous structure.

The SEM and TEM images in Figure 4 indicate that uniform $MnFe_2O_4$ (Figure 4a,b), $CoFe_2O_4$ (Figure 4c,d), $Mn_{0.25}Co_{0.75}Fe_2O_4$ (Figure 4e,f), and $Mn_{0.75}Co_{0.25}Fe_2O_4$ (Figure 4g,h) yolk bishell hollow microspheres are prepared after the crystallization and annealing treatment, and the XRD patterns in Figure S7 in the Supporting Information show the observation of the diffraction peaks at 2θ values of about 30.2, 35.6, 43.4, 57.4, and 62.8° that correspond to the lattice planes of (220), (311), (400), (511), and (440), respectively, indicating the formation of $MnFe_2O_4$ (Figure S7a in the Supporting Information), $CoFe_2O_4$ (Figure S7b in the Supporting Information), $Mn_{0.5}Co_{0.5}Fe_2O_4$ (Figure S7c in the Supporting Information), $Mn_{0.75}Co_{0.25}Fe_2O_4$ (Figure S7d in the Supporting Information), $Mn_{0.25}Co_{0.75}Fe_2O_4$ (Figure S7e in the Supporting Information) yolk bishell hollow microspheres, and $Mn_{0.5}Co_{0.5}Fe_2O_4$/carbon microspheres (Figure S7f in the Supporting Information). A calculation over the (311) reflection using the classical Scherrer equation from XRD patterns shows that the average crystallite diameters of these samples are about 9.3−13.2 nm, respectively. In addition, the

DOI: 10.1021/acsami.5b00617
ACS Appl. Mater. Interfaces 2015, 7, 6300−6309

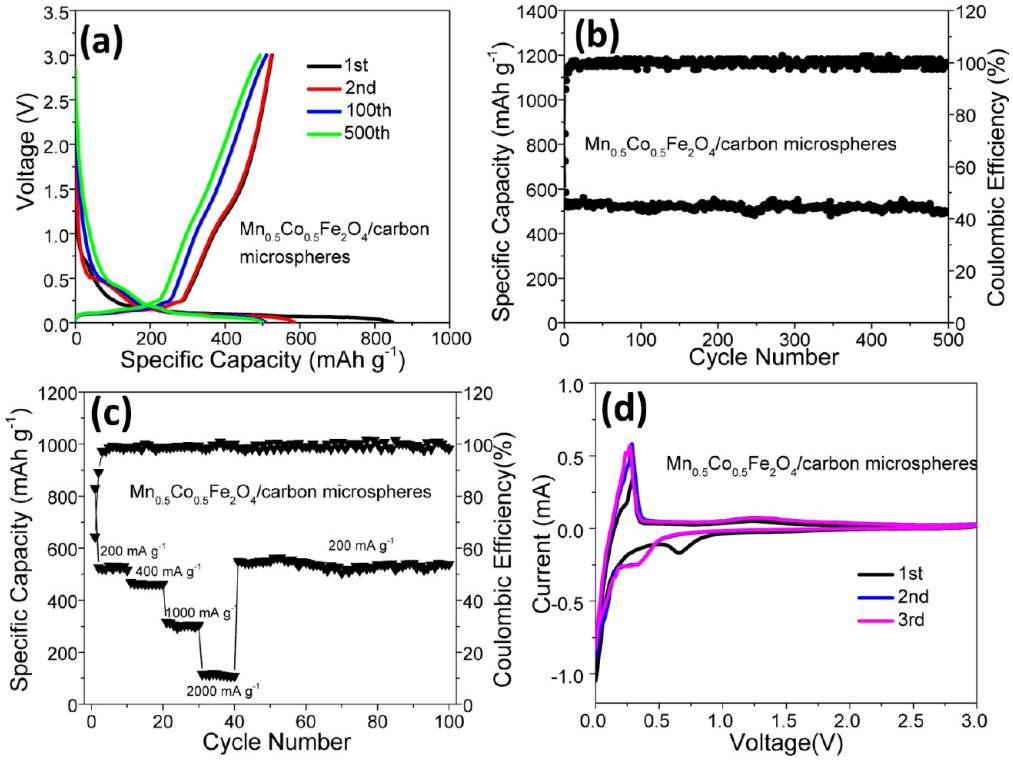

Figure 6. Electrochemical properties: the discharge−charge curves of the first, second, 100th, and 500th cycles (a), cycling property and Coulombic efficiency at a current density of 200 mA g^{-1} (b), rate performance at different current densities (c), and CV curves of the first three cycles at a scan rate of 0.1 mV s^{-1} (d) for $Mn_{0.5}Co_{0.5}Fe_2O_4$/carbon microspheres.

strong (002) peak at 2θ values of about 26.3° is observed for the $Mn_{0.5}Co_{0.5}Fe_2O_4$/carbon microspheres, proving the presence of carbon. The EDX spectra in Figure S8 in the Supporting Information further confirm the elemental compositions of $MnFe_2O_4$ (Figure S8a in the Supporting Information), $CoFe_2O_4$ (Figure S8b in the Supporting Information), $Mn_{0.5}Co_{0.5}Fe_2O_4$ (Figure S8c in the Supporting Information), $Mn_{0.75}Co_{0.25}Fe_2O_4$ (Figure S8d in the Supporting Information), $Mn_{0.25}Co_{0.75}Fe_2O_4$ (Figure S8e in the Supporting Information) yolk bishell hollow microspheres, while the TEM images in Figure S9 in the Supporting Information show that $MnFe_2O_4$ (Figure S9a in the Supporting Information), $CoFe_2O_4$ (Figure S9b in the Supporting Information), $Mn_{0.25}Co_{0.75}Fe_2O_4$ (Figure S9c in the Supporting Information), $Mn_{0.75}Co_{0.25}Fe_2O_4$ (Figure S9d in the Supporting Information) yolk−shell hollow microspheres are synthesized after the direct crystallization-annealing treatment.

Figure 5a shows the wide XPS spectra of $Mn_{0.5}Co_{0.5}Fe_2O_4$ yolk bishell hollow microspheres, revealing the presence of Mn, Co, Fe, and O elements. The Mn 2p spectrum (Figure 5b) indicates that two strong peaks at 641.2 eV for Mn $2p^{3/2}$ and 653.1 eV for Mn $2p^{1/2}$ are observed, indicating the oxidation state of Mn^{2+} in $Mn_{0.5}Co_{0.5}Fe_2O_4$. In the Co 2p spectrum shown in Figure 5c, two strong peaks at 780.5 eV assigned to Co $2p_{3/2}$ and 796.1 eV to Co $2p_{1/2}$ and two shakeup satellites (indicated as "Sat.") are observed, indicating the oxidation state of Co^{2+} in $Mn_{0.5}Co_{0.5}Fe_2O_4$. Figure 5d indicates the observation of two major peaks at 710.7 and 724.4 eV and two shakeup satellites, which can be ascribed to Fe $2p^{3/2}$ and Fe $2p^{1/2}$ of Fe^{3+}, respectively. In addition, the atomic ratio of Mn, Co, and Fe elements is approximately 1:1:4 from ICP-OES analysis.

The electrochemical properties of the $Mn_{0.5}Co_{0.5}Fe_2O_4$/carbon microspheres, $Mn_{0.5}Co_{0.5}Fe_2O_4$ yolk bishell and yolk−shell hollow microspheres toward the lithium storage are shown in Figure 6 and Figure S8d in the Supporting Information. Figure 6a indicates the discharge−charge curves of the first, second, 100th, and 500th cycles for $Mn_{0.5}Co_{0.5}Fe_2O_4$/carbon microspheres at a current density of 200 mA g^{-1}. The first discharge capacity is around 846.6 mAh g^{-1}, whereas the corresponding charge capacity is about 525.9 mAh g^{-1}. This corresponds to an initial Coulombic efficiency of 62.1%. These irreversible capacity losses can be attributed to the formation of the solid electrolyte interface layer[52] and the side reactions during the electrochemical process.[53] The discharge−charge curves for the second, 100th and 500th cycles almost coincide with each other, indicating the good cycling stability. The discharge−charge capacity for the $Mn_{0.5}Co_{0.5}Fe_2O_4$ component may be based on the oxidation−reduction of metallic Fe, Co, and Mn nanoparticles to $Mn_{0.5}Co_{0.5}Fe_2O_4$ via the reaction: $4Li_2O + 0.5Mn + 0.5Co + 2Fe \leftrightarrow Mn_{0.5}Co_{0.5}Fe_2O_4 + 8Li^+ + 8e^-$. A distinct voltage plateau can be clearly identified at ∼1.0−1.5 V, which is corresponding to the reduction of Fe^{3+} to Fe, Co^{2+} to Co, and Mn^{2+} to Mn during the initial discharge process. Meanwhile, a clear plateau is observed in the charge process at ∼0.2−0.5 V, which is corresponding to the oxidation of Fe to Fe^{3+}, Co to Co^{2+}, and Mn to Mn^{2+} during the initial charge process. The discharge voltage plateau of $Mn_{0.5}Co_{0.5}Fe_2O_4$/carbon microspheres is lower than that of the $Mn_{0.5}Co_{0.5}Fe_2O_4$ yolk bishell hollow microspheres (Figure S10a in the Supporting Information), probably because the carbon has a lower discharge voltage plateau.[5,54]

After 500 cycles, the discharge capacity of $Mn_{0.5}Co_{0.5}Fe_2O_4$/carbon microspheres measured at the current density of 200 mA g^{-1} still maintains at about 498.3 mAh g^{-1}, as shown in Figure 6b, which is very stable with almost 94.7% capacity retention. From the corresponding Coulombic efficiency curve

DOI: 10.1021/acsami.5b00617
ACS Appl. Mater. Interfaces 2015, 7, 6300−6309

shown in Figure 6b, the Coulombic efficiency quickly reaches a value higher than 99% after several cycles. This cycling performance is remarkable better than that of the reported multishelled Co_3O_4 hollow microspheres,[46] Fe_2O_3 nanoflakes,[55] Fe_2O_3@carbon composites,[56] carbon-coated $CoMn_2O_4$ triple-shelled hollow spheres,[21] Fe_3O_4 nanoparticles embedded in a porous carbon matrix,[15] $Mn_{0.5}Co_{0.5}Fe_2O_4$ yolk−shell (a capacity of 577.8 mAh g^{-1} with almost 46.3% capacity retention for 100 cycles) and yolk bishell (a capacity of 774.6 mAh g^{-1} with almost 59.1% capacity retention for 100 cycles) hollow microspheres (Figure S10b in the Supporting Information). Figure 6c displays the rate performance of the $Mn_{0.5}Co_{0.5}Fe_2O_4$/carbon microspheres measured at different current densities. The measured discharge capacities are about 830.6, 468.7, 316.8, 115.3, and 550.6 mAh g^{-1}, at the current density of 200, 400, 1000, 2000, and 200 mA g^{-1}, and the retention of the capacity is around 98.2, 98.8, 96.2, 94.3, and 97.7% after 10, 10, 10, 10, and 60 cycles, respectively, indicating the good rate performance. The excellent cycling stability and rate performance of $Mn_{0.5}Co_{0.5}Fe_2O_4$/carbon microspheres could be attributed to the formed nanostructured metal oxide particles with a small size that can partially buffer the stress and strain effects caused by the particle volume expansion/contraction during the Li-ion insertion/extraction.[57] Figure 6d presents the cyclic voltammetry (CV) curves of the $Mn_{0.5}Co_{0.5}Fe_2O_4$/carbon microspheres for the first three cycles at a scan rate of 0.1 mV s^{-1}, respectively. In the first scan, one cathodic peak is observed at about 0.50−0.85 V, which corresponds to the conversion reactions of Fe^{3+}, Co^{2+}, and Mn^{2+} to their metallic states and the formation of Li_2O, respectively. The weak broad anodic peak from 1.12 to 1.62 V can be ascribed to the oxidation reactions of metallic Fe, Co, and Mn. The metal oxide $Mn_{0.5}Co_{0.5}Fe_2O_4$ stores Li through reversible formation and decomposition of Li_2O. The observation of the strong cathodic peak below 0.20 V and anodic peak at about 0.18−0.51 V suggests the insertion/extraction of lithium ions from carbon. In the second and third scans, the reduction peak is shifted to 0.16−0.50 V. The peak intensity and integral areas of the second and third cycles are almost the same, revealing the good reversible oxidation−reduction reaction, reversible formation and decomposition of Li_2O, and the insertion and extraction of lithium ions from carbon, respectively. Because of the presence of the carbon network, the $Mn_{0.5}Co_{0.5}Fe_2O_4$/carbon microspheres exhibit lower electric resistance than the $Mn_{0.5}Co_{0.5}Fe_2O_4$ yolk bishell and yolk−shell hollow microspheres, as evidenced by the reduced diameter of these semicircle at high-frequency region in the electrochemical impedance spectroscopy (EIS) patterns (Figure S11 in the Supporting Information). After 500 discharge−charge cycles, the SEM image of the electrode disks containing charged $Mn_{0.5}Co_{0.5}Fe_2O_4$/carbon microspheres composites (Figure S12a in the Supporting Information) show that the original textural properties of these materials are still well-retained, and thin SEI layers (Figure S12b in the Supporting Information) on the surface of the $Mn_{0.5}Co_{0.5}Fe_2O_4$/carbon microspheres are observed, indicating the good structural stability of these materials. The carbon microspheres can strengthen the mechanical stability of the $Mn_{0.5}Co_{0.5}Fe_2O_4$/carbon composites, and absorb the volume change during the discharge−charge processes.[58,59] Moreover, the carbon network can certainly enhance the electrical conductivity of metal oxides after the thermal annealing treatment, which could contribute to the rate performance.[60,61]

4. CONCLUSIONS

In summary, the $Mn_xCo_{1-x}Fe_2O_4$ ($0 \le x \le 1$) yolk bishell hollow microspheres have been prepared through a template synthesis followed with an "adsorption, crystallization, and annealing" treatment. In comparison with the bare $Mn_{0.5}Co_{0.5}Fe_2O_4$ sample, the obtained $Mn_{0.5}Co_{0.5}Fe_2O_4$/carbon microspheres with $Mn_{0.5}Co_{0.5}Fe_2O_4$ nanoparticles homogeneously distributed in the carbon network exhibit a high capacity of 498.3 mAh g^{-1} at 200 mA g^{-1} even after 500 cycles, making them promising for the next generation lithium-ion batteries. This work opens a new way for fabrication of transition metal oxides/carbon microspheres as anodes for lithium-ion batteries with long cycling life. In addition, it is expected that the fabricated transition metal oxides yolk bishell hollow microspheres will have applications in the nanoreactor, catalyst, drug delivery, and solar cells.

■ ASSOCIATED CONTENT

Supporting Information

Additional characterization data, such as SEM and TEM images, EDX spectroscopy, XRD patterns, TG curves, N_2 adsorption−desorption isotherms, and electrochemical properties, are shown in Figures S1−S12 and Table S1. This material is available free of charge via the Internet at http://pubs.acs.org.

■ AUTHOR INFORMATION

Corresponding Authors

*E-mail: zhangzl@ipe.ac.cn. Phone: +86-10-82544850, Fax: +86-10-82544851.
*E-mail: qtan@ipe.ac.cn.
*E-mail: fbsu@ipe.ac.cn.

Notes

The authors declare no competing financial interest.

■ ACKNOWLEDGMENTS

The authors gratefully acknowledge the supports from the National Natural Science Foundation of China (Grants 51402299, 21031005, and 51272252) and the Hundred Talents Program of the Chinese Academy of Sciences.

■ REFERENCES

(1) Mann, M. E.; Bradley, R. S.; Hughes, M. K. Global-Scale Temperature Patterns and Climate Forcing over the Past Six Centuries. *Nature* **1998**, *392*, 779.
(2) Virkutyte, J.; Varma, R. S. Green Synthesis of Metal Nanoparticles: Biodegradable Polymers and Enzymes in Stabilization and Surface Functionalization. *Chem. Sci.* **2011**, *2*, 837.
(3) Liu, B. R.; Soares, P.; Checkles, C.; Zhao, Y.; Yu, G. H. Three-Dimensional Hierarchical Ternary Nanostructures for High-Performance Li-Ion Battery Anodes. *Nano Lett.* **2013**, *13*, 3414.
(4) Tarascon, J. M.; Armand, M. Issues and Challenges Facing Rechargeable Lithium Batteries. *Nature* **2001**, *414*, 359.
(5) Reddy, M. V.; Rao, G. V. S.; Chowdari, B. V. R. Metal Oxides and Oxysalts as Anode Materials for Li Ion Batteries. *Chem. Rev.* **2013**, *113*, 5364.
(6) Reed, J.; Ceder, G. Role of Electronic Structure in the Susceptibility of Metastable Transition-Metal Oxide Structures to Transformation. *Chem. Rev.* **2004**, *104*, 4513.
(7) Sasidharan, M.; Gunawardhana, N.; Yoshio, M.; Nakashima, K. Alpha-Fe_2O_3 and Fe_3O_4 Hollow Nanospheres as High-Capacity Anode Materials for Rechargeable Li-Ion Batteries. *Ionics* **2013**, *19*, 25.
(8) Tummala, R.; Guduru, R. K.; Mohanty, P. S. Binder Free, Porous and Nanostructured Co_3O_4 Anode for Li-Ion Batteries from Solution Precursor Plasma Deposition. *J. Power Sources* **2012**, *199*, 270.

DOI: 10.1021/acsami.5b00617
ACS Appl. Mater. Interfaces 2015, 7, 6300−6309

(9) Yue, J.; Gu, X.; Chen, L.; Wang, N. N.; Jiang, X. L.; Xu, H. Y.; Yang, J.; Qian, Y. T. General Synthesis of Hollow MnO_2, Mn_3O_4 and MnO Nanospheres as Superior Anode Materials for Lithium Ion Batteries. *J. Mater. Chem. A* **2014**, *2*, 17421.
(10) Li, J. F.; Xiong, S. L.; Li, X. W.; Qian, Y. T. A Facile Route to Synthesize Multiporous $MnCo_2O_4$ and $CoMn_2O_4$ Spinel Quasi-Hollow Spheres with Improved Lithium Storage Properties. *Nanoscale* **2013**, *5*, 2045.
(11) Zhang, Z.; Wang, Y.; Tan, Q.; Zhong, Z.; Su, F. Facile Solvothermal Synthesis of Mesoporous Manganese Ferrite ($MnFe_2O_4$) Microspheres as Anode Materials for Lithium-Ion Batteries. *J. Colloid Interface Sci.* **2013**, *398*, 185.
(12) Poizot, P.; Laruelle, S.; Grugeon, S.; Dupont, L.; Tarascon, J. M. Nano-Sized Transition-Metal Oxides as Negative-Electrode Materials for Lithium-Ion Batteries. *Nature* **2000**, *407*, 496.
(13) Choi, S. H.; Kang, Y. C. Yolk-Shell, Hollow, and Single-Crystalline $ZnCo_2O_4$ Powders: Preparation Using a Simple One-Pot Process and Application in Lithium-Ion Batteries. *ChemSusChem* **2013**, *6*, 2111.
(14) Wu, H. B.; Chen, J. S.; Hng, H. H.; Lou, X. W. Nanostructured Metal Oxide-Based Materials as Advanced Anodes for Lithium-Ion Batteries. *Nanoscale* **2012**, *4*, 2526.
(15) Latorre-Sanchez, M.; Primo, A.; Garcia, H. Green Synthesis of Fe_3O_4 Nanoparticles Embedded in a Porous Carbon Matrix and Its Use as Anode Material in Li-Ion Batteries. *J. Mater. Chem.* **2012**, *22*, 21373.
(16) Park, J.; Moon, W. G.; Kim, G. P.; Nam, I.; Park, S.; Kim, Y.; Yi, J. Three-Dimensional Aligned Mesoporous Carbon Nanotubes Filled with Co_3O_4 Nanoparticles for Li-Ion Battery Anode Applications. *Electrochim. Acta* **2013**, *105*, 110.
(17) Xia, Y.; Xiao, Z.; Dou, X.; Huang, H.; Lu, X. H.; Yan, R. J.; Gan, Y. P.; Zhu, W. J.; Tu, J. P.; Zhang, W. K.; Tao, X. Y. Green and Facile Fabrication of Hollow Porous MnO/C Microspheres from Microalgaes for Lithium-Ion Batteries. *ACS Nano* **2013**, *7*, 7083.
(18) Xie, Q. S.; Zhang, X. Q.; Wu, X. B.; Wu, H. Y.; Liu, X.; Yue, G. H.; Yang, Y.; Peng, D. L. Yolk-Shell ZnO-C Microspheres with Enhanced Electrochemical Performance as Anode Material for Lithium Ion Batteries. *Electrochim. Acta* **2014**, *125*, 659.
(19) Xie, Q. S.; Ma, Y. T.; Zeng, D. Q.; Zhang, X. Q.; Wang, L. S.; Yue, G. H.; Peng, D. L. Hierarchical ZnO-Ag-C Composite Porous Microspheres with Superior Electrochemical Properties as Anode Materials for Lithium Ion Batteries. *ACS Appl. Mater. Interfaces* **2014**, *6*, 19895.
(20) Zhang, Z.; Wang, Y.; Zhang, M.; Tan, Q.; Lv, X.; Zhong, Z.; Su, F. Mesoporous $CoFe_2O_4$ Nanospheres Cross-Linked by Carbon Nanotubes as High-Performance Anodes for Lithium-Ion Batteries. *J. Mater. Chem. A* **2013**, *1*, 7444.
(21) Zhang, G. Q.; Lou, X. W. General Synthesis of Multi-Shelled Mixed Metal Oxide Hollow Spheres with Superior Lithium Storage Properties. *Angew. Chem., Int. Ed.* **2014**, *53*, 9041.
(22) Wang, Z. Y.; Wang, Z. C.; Liu, W. T.; Xiao, W.; Lou, X. W. Amorphous $CoSnO_3$@C Nanoboxes with Superior Lithium Storage Capability. *Energy Environ. Sci.* **2013**, *6*, 87.
(23) Ko, Y. N.; Park, S. B.; Kang, Y. C. Design and Fabrication of New Nanostructured SnO_2-Carbon Composite Microspheres for Fast and Stable Lithium Storage Performance. *Small* **2014**, *10*, 3240.
(24) Tao, S. S.; Yue, W. B.; Zhong, M. Y.; Chen, Z. J.; Ren, Y. Fabrication of Graphene-Encapsulated Porous Carbon-Metal Oxide Composites as Anode Materials for Lithium-Ion Batteries. *ACS Appl. Mater. Interfaces* **2014**, *6*, 6332.
(25) Yuan, C. Z.; Wu, H. B.; Xie, Y.; Lou, X. W. Mixed Transition-Metal Oxides: Design, Synthesis, and Energy-Related Applications. *Angew. Chem., Int. Ed.* **2014**, *53*, 1488.
(26) Cao, L.; Chen, D. H.; Caruso, R. A. Surface-Metastable Phase-Initiated Seeding and Ostwald Ripening: A Facile Fluorine-Free Process towards Spherical Fluffy Core/Shell, Yolk/Shell, and Hollow Anatase Nanostructures. *Angew. Chem., Int. Ed.* **2013**, *52*, 10986.
(27) Liu, J.; Qiao, S. Z.; Chen, J. S.; Lou, X. W.; Xing, X. R.; Lu, G. Q. Yolk/Shell Nanoparticles: New Platforms for Nanoreactors, Drug Delivery and Lithium-Ion Batteries. *Chem. Commun.* **2011**, *47*, 12578.
(28) Wu, X. J.; Xu, D. S. Soft Template Synthesis of Yolk/Silica Shell Particles. *Adv. Mater.* **2010**, *22*, 1516.
(29) Guan, B. Y.; Wang, X.; Xiao, Y.; Liu, Y. L.; Huo, Q. S. A Versatile Cooperative Template-Directed Coating Method to Construct Uniform Microporous Carbon Shells for Multifunctional Core-Shell Nanocomposites. *Nanoscale* **2013**, *5*, 2469.
(30) Hu, M.; Belik, A. A.; Imura, M.; Yamauchi, Y. Tailored Design of Multiple Nanoarchitectures in Metal-Cyanide Hybrid Coordination Polymers. *J. Am. Chem. Soc.* **2013**, *135*, 384.
(31) Wang, Z. Y.; Zhou, L.; Lou, X. W. Metal Oxide Hollow Nanostructures for Lithium-ion Batteries. *Adv. Mater.* **2012**, *24*, 1903.
(32) Yin, Y. D.; Rioux, R. M.; Erdonmez, C. K.; Hughes, S.; Somorjai, G. A.; Alivisatos, A. P. Formation of Hollow Nanocrystals through the Nanoscale Kirkendall Effect. *Science* **2004**, *304*, 711.
(33) Li, H. X.; Bian, Z. F.; Zhu, J.; Zhang, D. Q.; Li, G. S.; Huo, Y. N.; Li, H.; Lu, Y. F. Mesoporous Titania Spheres with Tunable Chamber Stucture and Enhanced Photocatalytic Activity. *J. Am. Chem. Soc.* **2007**, *129*, 8406.
(34) Guan, B. Y.; Wang, T.; Zeng, S. J.; Wang, X.; An, D.; Wang, D. M.; Cao, Y.; Ma, D. X.; Liu, Y. L.; Huo, Q. S. A Versatile Cooperative Template-Directed Coating Method to Synthesize Hollow and Yolk-Shell Mesoporous Zirconium Titanium Oxide Nanospheres as Catalytic Reactors. *Nano Res.* **2014**, *7*, 246.
(35) Li, G. L.; Mohwald, H.; Shchukin, D. G. Precipitation Polymerization for Fabrication of Complex Core-Shell Hybrid Particles and Hollow Structures. *Chem. Soc. Rev.* **2013**, *42*, 3628.
(36) Li, W.; Deng, Y. H.; Wu, Z. X.; Qian, X. F.; Yang, J. P.; Wang, Y.; Gu, D.; Zhang, F.; Tu, B.; Zhao, D. Y. Hydrothermal Etching Assisted Crystallization: A Facile Route to Functional Yolk-Shell Titanate Microspheres with Ultrathin Nanosheets-Assembled Double Shells. *J. Am. Chem. Soc.* **2011**, *133*, 15830.
(37) Liu, Y. D.; Goebl, J.; Yin, Y. D. Templated Synthesis of Nanostructured Materials. *Chem. Soc. Rev.* **2013**, *42*, 2610.
(38) Lai, X. Y.; Halpert, J. E.; Wang, D. Recent Advances in Micro-/nano-Structured Hollow Spheres for Energy Applications: From Simple to Complex Systems. *Energy Environ. Sci.* **2012**, *5*, 5604.
(39) Caruso, R. A.; Susha, A.; Caruso, F. Multilayered Titania, Silica, and Laponite Nanoparticle Coatings on Polystyrene Colloidal Templates and Resulting Inorganic Hollow Spheres. *Chem. Mater.* **2001**, *13*, 400.
(40) Kwon, K. A.; Lim, H. S.; Sun, Y. K.; Suh, K. D. Alpha-Fe_2O_3 Submicron Spheres with Hollow and Macroporous Structures as High-Performance Anode Materials for Lithium Ion Batteries. *J. Phys. Chem. C* **2014**, *118*, 2897.
(41) Kang, N.; Park, J. H.; Jin, M.; Park, N.; Lee, S. M.; Kim, H. J.; Kim, J. M.; Son, S. U. Microporous Organic Network Hollow Spheres: Useful Templates for Nanoparticulate Co_3O_4 Hollow Oxidation Catalysts. *J. Am. Chem. Soc.* **2013**, *135*, 19115.
(42) Tang, X. H.; Liu, Z. H.; Zhang, C. X.; Yang, Z. P.; Wang, Z. L. Synthesis and Capacitive Property of Hierarchical Hollow Manganese Oxide Nanospheres with Large Specific Surface Area. *J. Power Sources* **2009**, *193*, 939.
(43) Qian, H. S.; Lin, G. F.; Zhang, Y. X.; Gunawan, P.; Xu, R. A New Approach to Synthesize Uniform Metal Oxide Hollow Nanospheres via Vontrolled Precipitation. *Nanotechnology* **2007**, *18*, 355602.
(44) Xu, S. M.; Hessel, C. M.; Ren, H.; Yu, R. B.; Jin, Q.; Yang, M.; Zhao, H. J.; Wang, D. Alpha-Fe_2O_3 Multi-Shelled Hollow Microspheres for Lithium Ion Battery Anodes with Superior Capacity and Charge Retention. *Energy Environ. Sci.* **2014**, *7*, 632.
(45) Li, S. L.; Li, A. H.; Zhang, R. R.; He, Y. Y.; Zhai, Y. J.; Xu, L. Q. Hierarchical Porous Metal Ferrite Ball-in-Ball Hollow Spheres: General Synthesis, Formation Mechanism, and High Performance as Anode Materials for Li-Ion Batteries. *Nano Res.* **2014**, *7*, 1116.
(46) Wang, J. Y.; Yang, N. L.; Tang, H. J.; Dong, Z. H.; Jin, Q.; Yang, M.; Kisailus, D.; Zhao, H. J.; Tang, Z. Y.; Wang, D. Accurate Control of Multishelled Co_3O_4 Hollow Microspheres as High-Performance

DOI: 10.1021/acsami.5b00617
ACS Appl. Mater. Interfaces 2015, 7, 6300−6309

Anode Materials in Lithium-Ion Batteries. *Angew. Chem., Int. Ed.* **2013**, *52*, 6417.
(47) Jiang, J.; Li, Y. Y.; Liu, J. P.; Huang, X. T.; Yuan, C. Z.; Lou, X. W. Recent Advances in Metal Oxide-Based Electrode Architecture Design for Electrochemical Energy Storage. *Adv. Mater.* **2012**, *24*, 5166.
(48) Sun, X. M.; Li, Y. D. Colloidal Carbon Spheres and Their Core/Shell Structures with Noble-Metal Nanoparticles. *Angew. Chem., Int. Ed.* **2004**, *43*, 597.
(49) Qian, H. S.; Yu, S. H.; Luo, L. B.; Gong, J. Y.; Fei, L. F.; Liu, X. M. Synthesis of Uniform Te@Carbon-Rich Composite Nanocables with Photoluminescence Properties and Carbonaceous Nanofibers by the Hydrothermal Varbonization of Glucose. *Chem. Mater.* **2006**, *18*, 2102.
(50) Zhang, G. Q.; Yu, L.; Wu, H. B.; Hoster, H. E.; Lou, X. W. Formation of $ZnMn_2O_4$ Ball-in-Ball Hollow Microspheres as a High-Performance Anode for Lithium-Ion Batteries. *Adv. Mater.* **2012**, *24*, 4609.
(51) Jagadeesan, D.; Mansoori, U.; Mandal, P.; Sundaresan, A.; Eswaramoorthy, M. Hollow Spheres to Nanocups: Tuning the Morphology and Magnetic Properties of Single-Crystalline Alpha-Fe_2O_3 Nanostructures. *Angew. Chem., Int. Ed.* **2008**, *47*, 7685.
(52) Qi, Y.; Zhang, H.; Du, N.; Yang, D. R. Highly Loaded CoO/Graphene Nanocomposites as Lithium-Ion Anodes with Superior Reversible Capacity. *J. Mater. Chem. A* **2013**, *1*, 2337.
(53) Zhang, Z.; Ren, W.; Wang, Y.; Yang, J.; Tan, Q.; Zhong, Z.; Su, F. $Mn_{0.5}Co_{0.5}Fe_2O_4$ Nanoparticles Highly Dispersed in Porous Carbon Microspheres as High Performance Anode Materials in Li-Ion Batteries. *Nanoscale* **2014**, *6*, 6805.
(54) Shi, W. H.; Rui, X. H.; Zhu, J. X.; Yan, Q. Y. Design of Nanostructured Hybrid Materials Based on Carbon and Metal Oxides for Li Ion Batteries. *J. Phys. Chem. C* **2012**, *116*, 26685.
(55) Reddy, M. V.; Yu, T.; Sow, C. H.; Shen, Z. X.; Lim, C. T.; Rao, G. V. S.; Chowdari, B. V. R. Alpha-Fe_2O_3 Nanoflakes as an Anode Material for Li-Ion Batteries. *Adv. Funct. Mater.* **2007**, *17*, 2792.
(56) Oh, H. D.; Lee, S. W.; Kim, S. O.; Lee, J. K. Facile Synthesis of Carbon Layer-Entangled Fe_2O_3 Clusters as Anode Materials for Improved Li-Ion Batteries. *J. Power Sources* **2013**, *244*, 575.
(57) Bueno, P. R.; Leite, E. R. Nanostructured Li Ion Insertion Electrodes. 1. Discussion on Fast Transport and Short Path for Ion Diffusion. *J. Phys. Chem. B* **2003**, *107*, 8868.
(58) Zhang, H. W.; Zhou, L.; Noonan, O.; Martin, D. J.; Whittaker, A. K.; Yu, C. Z. Tailoring the Void Size of Iron Oxide@Carbon Yolk-Shell Structure for Optimized Lithium Storage. *Adv. Funct. Mater.* **2014**, *24*, 4337.
(59) Sun, X. F.; Xu, Y. L.; Ding, P.; Chen, G. G.; Zheng, X. Y.; Zhang, R.; Li, L. The Composite Sphere of Manganese Oxide and Carbon Nanotubes as a Prospective Anode Material for Lithium-Ion Batteries. *J. Power Sources* **2014**, *255*, 163.
(60) Lei, C.; Han, F.; Sun, Q.; Li, W. C.; Lu, A. H. Confined Nanospace Pyrolysis for the Fabrication of Coaxial Fe_3O_4@C Hollow Particles with a Penetrated Mesochannel as a Superior Anode for Li-Ion Batteries. *Chem.—Eur. J.* **2014**, *20*, 139.
(61) Su, Y. Z.; Li, S.; Wu, D. Q.; Zhang, F.; Liang, H. W.; Gao, P. F.; Cheng, C.; Feng, X. L. Two-Dimensional Carbon-Coated Graphene/Metal Oxide Hybrids for Enhanced Lithium Storage. *ACS Nano* **2012**, *6*, 8349.

DOI: 10.1021/acsami.5b00617
ACS Appl. Mater. Interfaces 2015, 7, 6300−6309